Office of Naval Research

Contract Nonr-1866(28)

NR - 372 - 013

Technical Report

on

A 21-CENTIMETER TRAVELING-WAVE MASER

by

E. B. Treacy

January 22, 1963

The research reported in this document was made possible through support extended Cruft Laboratory, Harvard University, jointly by the Navy Department (Office of Naval Research), the Signal Corps of the U. S. Army, and the U. S. Air Force, under ONR Contract Nonr-1866 (28). Reproduction in whole or in part is permitted for any purpose of the United States Government.

Technical Report No. 401

Cruft Laboratory

Harvard University

Cambridge, Massachusetts

405055

ABSTRACT

A traveling-wave maser tunable over the frequency range of 1340 Mc to 1430 Mc has been developed and constructed for use in radio astronomical research. It uses ruby as the maser material and a comb as the slow-wave structure. The net gain exceeds 30 dB over most of its tuning range, while the average instantaneous bandwidth is about 11 Mc. It has been designed for operation at 4.2°K.

A

A 21-CENTIMETER TRAVELING-WAVE MASER FOR THE HARVARD RADIO TELESCOPE

by

E. B. Treacy

Division of Engineering and Applied Physics

Harvard University, Cambridge, Massachusetts

I. Introduction

The study of the radiation emitted by neutral hydrogen in its ground electronic state has proved to be a most valuable contribution to astronomy in recent years. The spectral line occurs at 1420.4 Mc and has been observed in both emission and absorption. The cold neutral hydrogen cannot be observed optically, yet it comprises a significant fraction of the matter in the universe. Its distribution in many cases tends to be similar to that of the stars, which are formed from it. Observation of the neutral hydrogen in our galaxy by radio astronomy has established the existence of spiral structure [1], which has been mapped out fairly extensively. Hydrogen line studies of external galaxies yield valuable information to supplement optical observations.

The natural width of the hydrogen line emission is extremely small and collisions between atoms are rare, so that the observed linewidth is due mainly to Doppler broadening and is, typically, of the order of tens of kilocycles for a cloud. The Doppler shift due to the radial component of motion of hydrogen is 4.73 kc per km/sec velocity. All galaxies external to the local

group show a red-shift, which is usually interpreted as being due to an expansion of the universe. The velocity of recession is about 180 km/sec per Mpc [2],corresponding to a Doppler shift of 851.4 kc/Mpc of the hydrogen line.

The application of a maser to radio astronomy was suggested by Bloembergen [3] in his original paper on the three-level maser. A 21 cm cavity maser was subsequently built in Gordon McKay Laboratory by Cooper and Jelley [4]. It has been operating very successfully during the past two and a half years at the focus of the 60 foot dish at the Harvard College Observatory Agassiz Station. The 21 cm hydrogen line emission from about two thirds of the galaxies so far studied was discovered first with this particular instrument [5] .

At the time of the construction of this instrument,it was realized that a traveling-wave maser would offer several advantages over the cavity type. These advantages are:

1. It avoids the use of a circulator (usually at 300°K) for separating the input and output, thus eliminating,typically, 20° from the input noise contribution.
2. It has larger instantaneous bandwidth.
3. It has better gain stability.
4. No mechanical tuning is required in changing the frequency.

The aim of the present project has been to develop such a traveling-wave maser and to package it in a form suitable for installation on the 60 foot dish. The cavity maser has a gain of 20 dB and bandwidth about 2 Mc. The type of characteristics a radio astronomer would like to have are gain, about 25 dB; instantaneous bandwidth, 10 to 20 Mc; tuning range, 1422 Mc down as far as one can go in the design. The operating temperature should be 4.2°K, i.e., liquid helium temperature at standard atmospheric pressure. Higher gain could be accomplished by pumping on the helium, but this is undesirable in that it adds to the complexity of the system, and introduces the possibility of gain instability (through pressure variations), as well as reducing the running time.

This report describes the TWM developed for the Harvard radio telescope.

II. Theory of Operation

The active material used is ruby with about .03 molar percentage of Cr_2O_3, and is operated with the c-axis at 90° to the magnetic field. The paramagnetic spectrum of ruby has been studied in great detail, and the pertinent results are summarized in a paper by Schulz - Du Bois [6]. Using the high-field notation of this reference, the signal transition is $-\overline{1}/2 \rightarrow -\overline{3}/2$, while the pump excites the $-\overline{3}/2 \rightarrow \overline{1}/2$ transition. For the signal transition at 1420 Mc, the magnetic field required is 1993 gauss, and this corresponds

to a pump frequency of 11.27 KMc. In this region the signal frequency changes at a rate of roughly 1.69 Mc/gauss while the pump frequency changes at a rate of about 2.60 Mc/gauss.

The polarization that gives maximum probability for the $-\overline{1}/2 \rightarrow -\overline{3}/2$ transition is elliptical in a plane at right angles to the external field with the major axis of the ellipse along the c-axis. Right and left circular polarizations will, therefore, both induce transitions. The relevant matrix elements for computing the transition probabilities have been tabulated by Chang and Siegman, and their tables are presented in a review article by Weber [7].

The table for H_o = 2000 oersteds and $\theta = 90^o$ is appropriate here. To use this table we note that Weber has tabulated the quantities α, β, and γ where

$$\frac{1}{\beta H_{rf}} < k \mid 2\beta \underset{\sim}{H}_{rf} \cdot \underset{\sim}{S} \mid \ell > = (\alpha, \phi_1 + \gamma \phi_3) + i\beta \phi_2 \qquad (1)$$

and (ϕ_1, ϕ_2, ϕ_3) are the direction cosines of H_{rf} with respect to a set of axes (X, Y, Z), where Z is in the c-axis direction. We need the matrix elements of S_x, S_y, and S_z, where x is along the c-axis and z in the direction of the external field, and we find them by dividing the entries for γ, β, and α respectively by two. The states 1, 2, 3, and 4 in Weber's article correspond to our $\mid \overline{3}/2 >$, $\mid \overline{1}/2 >$, $\mid -\overline{1}/2 >$ and $\mid -\overline{3}/2 >$ respectively.

We then find,

$$<-\overline{1}/2 \mid S_x \mid -\overline{3}/2> = 1.3268 = < -\overline{3}/2 \mid S_x \mid -\overline{1}/2 > \qquad (2a)$$

and

$$\langle -\bar{1}/2 \mid S_y \mid -\bar{3}/2 \rangle = -0.3427i = -\langle -\bar{3}/2 \mid S_y \mid -\bar{1}/2 \rangle . \quad (2b)$$

Therefore,

$$\langle -\bar{1}/2 \mid S_+ \mid -\bar{3}/2 \rangle = 1.6695 = \langle -\bar{3}/2 \mid S_- \mid -\bar{1}/2 \rangle \quad (3a)$$

and

$$\langle -\bar{1}/2 \mid S_- \mid -\bar{3}/2 \rangle = .9841 = \langle -\bar{3}/2 \mid S_+ \mid -\bar{1}/2 \rangle \quad (3b)$$

where

$$S_+ = S_x + iS_y$$

and

$$S_- = S_x - iS_y \quad .$$

The transition probabilities for the two circular polarizations are proportional to the quantities

$$| \langle -\bar{1}/2 \mid S_+ \mid -\bar{3}/2 \rangle |^2 = 2.79 \quad (4a)$$

and

$$| \langle -\bar{1}/2 \mid S_- \mid -\bar{3}/2 \rangle |^2 = .97 \quad , \quad (4b)$$

These may be compared to the squared matrix elements that would result in the absence of the crystal-field term in the Hamiltonian

$$| \langle 3/2 \mid S_+ \mid 1/2 \rangle |^2 = 3$$

$$| \langle 1/2 \mid S_+ \mid -1/2 \rangle |^2 = 4 \quad .$$

For linear polarization along the c-axis we have

$$| < -\overline{1}/2 | S_x | - \overline{3}/2 > |^2 = 1.75 \quad ,$$

while for linear polarization at right angles to both the c-axis and the external field we have

$$| < -\overline{1}/2 | S_y | -\overline{3}/2 > |^2 = 0.117 .$$

The polarization ellipse for maximum transition probability has its major and minor axes in the ratio of

$$\frac{|< -\overline{1}/2 | S_x | - \overline{3}/2 > |}{|< -\overline{1}/2 | S_y | - \overline{3}/2 > |} = 3.9 \qquad (5)$$

and the sense of polarization is, of course, that of a free electron.

For the pump transition, the same table gives $< -\overline{1}/2 | S_z | -\overline{3}/2 > = 0.88$, while the corresponding elements for S_x and S_y are zero. Optimum pumping, therefore, requires that the rf magnetic field be parallel to the external field.

The theory of operation of the TWM has been described by De Grasse, et. al. [8]. The present design represents an extension to lower frequencies of both the techniques described in that paper and those used in the development of the masers for "Project Echo", [9].

The basic principles of operation of a TWM are as follows. The signal is coupled into a slow-wave structure containing the ruby, which is activated by the pump power. The primary function of the structure is the storage of electromagnetic energy, which is essential for providing strong coupling between

the field and the ruby, since the transition probability is proportional to the square of the rf magnetic field. The "slow wave" property is a result of this energy storage. The structure is, therefore, a band-pass filter, and it can store energy at any frequency within its passband as contrasted to the cavity in which energy storage is a resonant phenomenon. Since the passband of the structure is larger than the paramagnetic resonance linewidth, the instantaneous amplifier bandwidth is determined by the latter, again in contrast with the cavity. (This leads to great gain stability.)

The slow wave structure used in this maser is a "comb" [8], the structure perfected by the Bell Telephone Laboratories group. The comb has the useful property of causing opposite senses of polarization on the two sides of the plane containing the periodically spaced elements (fingers). This permits the incorporation of an isolator into the structure. In brief, the maser consists of a comb loaded with ruby and other dielectric materials, and incorporates an isolator with high reverse loss.

In Ref. 8, the gain of a TWM is given by the formula

$$G = \text{cap}\left[-\frac{\omega F \chi''_{max} S\ell}{c}\right] \tag{6}$$

where ω is the angular frequency, S the slowing factor (velocity of light divided by the group velocity in the structure), ℓ the length of the structure, and c the velocity of light. The filling factor F is given by the relation

$$F = \frac{\int_{Am} H \cdot \chi'' \cdot H^{*} \, dS}{\chi''_{max} \int_{A_S} H^2 \, dS} \qquad (7)$$

where A_m is the cross-section area of the ruby and A_S is the cross-section area of the structure. χ'' is the imaginary part of the susceptibility tensor and χ''_{max} is the magnitude of the diagonalized χ'' tensor.

Compared to the TWM's described previously, the L-band maser gain is adversely affected by the factors ω and χ''_{max}, but the slowing factor S is greater for the same fractional bandwidth by the inverse frequency ratio. The net result is a decreased gain due to the decrease in χ''_{max}.

III. Description of Maser

The comb is made of copper and consists of 72 elements (fingers) each .040 x .040 x .830 [10] with a period between elements of .080 , and is situated midway between, and parallel to the wide walls of an X-band waveguide as shown in Fig. 1 . The inside dimensions of the waveguide are .900 x .260 . The total length of the comb is about 5 3/4 inches.

A cross-section view of the maser is shown in Fig. 2. The principal features to be noted in this diagram are:

(a) Ruby is placed on both sides of the comb structure.

(b) Isolator strips are placed on one side only, in the region where the rf magnetic field is strongest.

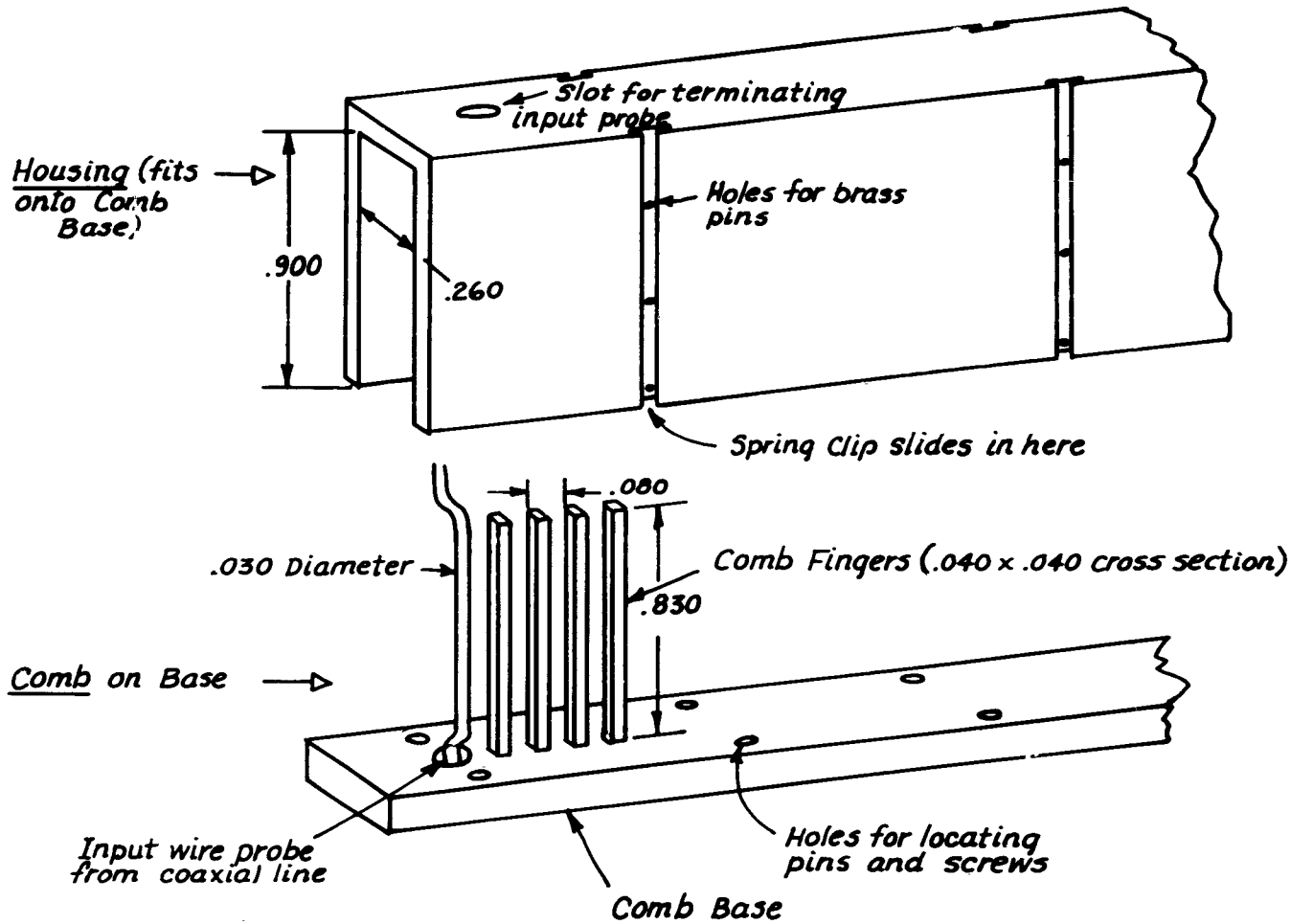

FIG. 1 THE COMB STRUCTURE

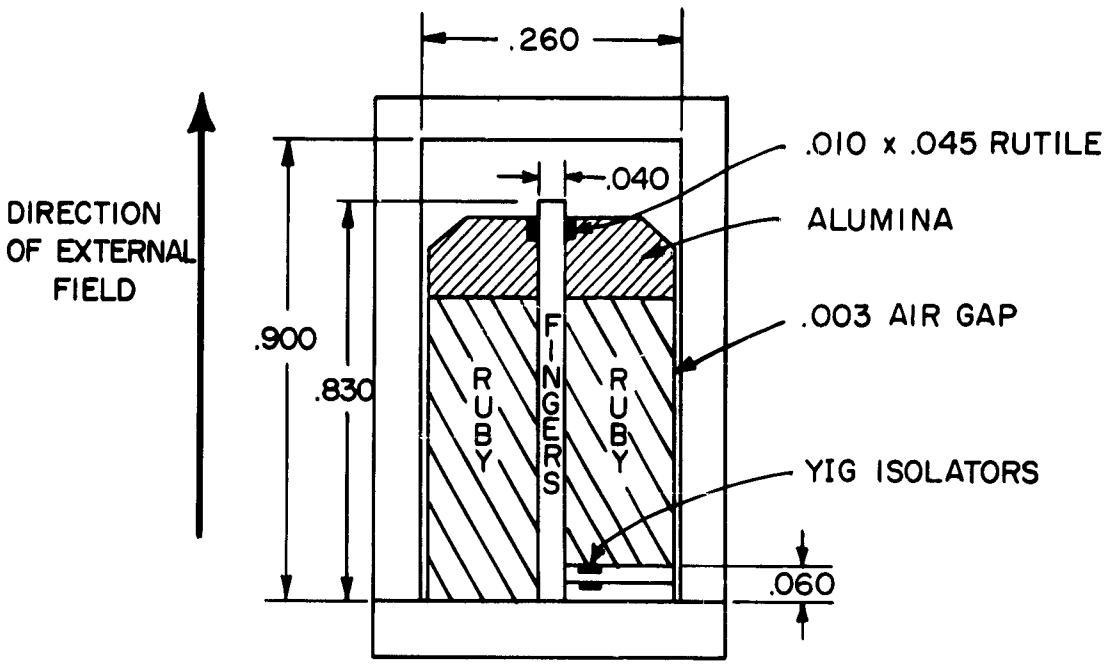

FIG. 2 CROSS SECTION OF MASER

(c) Shaped alumina pieces and polycrystalline rutile are used to fix certain properties associated with the wave propagation.

(d) There is an air space between the side walls and the ruby for ease in assembling the maser.

The external magnetic field is applied in the direction of the length of the fingers, while the rf magnetic fields due to propagation of the L-band signal are at right angles to this direction. The c-axis of the ruby also is perpendicular to the external field and would make an angle of about 60° with the plane of Fig. 2. Near the upper and lower cut-off frequencies of the fundamental passband of the structure the rf magnetic field is essentially linearly polarized, and both ruby pieces contribute about equally to the gain. Near the midband frequency the polarization of the field becomes more circular and the ruby pieces contributeroughly in the ratio 3:1 as one can see from Eq. 4 . Simple pictures of the rf fields are presented in Fig. 3 for three different values of rf phase shift between adjacent elements of the structure. The fields of Fig. 3A and 3B are non-propagating and so they are exponentially damped along the structure rather than uniform as shown in the diagrams.

The signal is coupled into the slow-wave structure from external coaxial lines by means of shaped wire probes near the end fingers, as shown in Fig. 1. The pump power is fed in from X-band waveguide joined to the end of the maser, and propagates down the structure in a complex

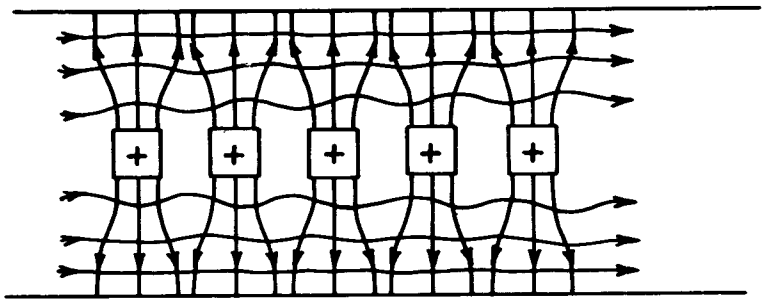

A. $\phi = 0$, Polarization is Linear everywhere.

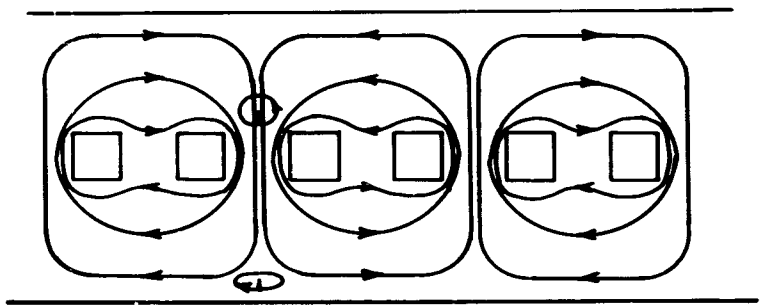

C. $\phi = \pi/2$, Magnetic Field only. Polarization Ellipses are shown also.

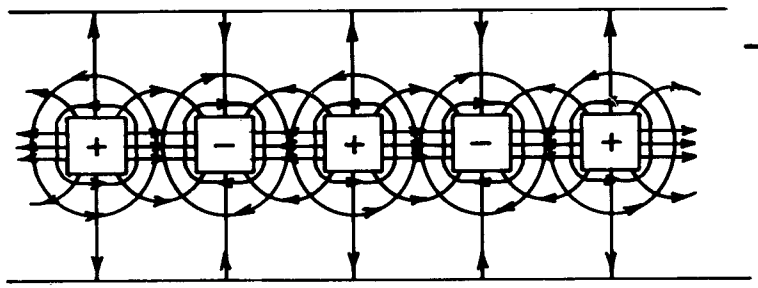

B. $\phi = \pi$, Polarization is Linear everywhere.

FIG. 3 FIELD DISTRIBUTIONS IN STRUCTURE FOR VARIOUS VALUES OF ϕ.

mode whose largest component is the TE_{10} . The maser presents a large discontinuity to the pumping signal and no real effort has been made to match the pump power into it. Experimentally, it is found that the power is coupled in resonantly at several frequencies within the linewidth of the pump transition, and this transition can be saturated with an available pump power of a few hundred milliwatts.

The isolator, as shown in Fig. 4, consists of pieces of polycrystalline YIG (yttrium iron garnet) of dimensions .040 x .040 x .004 [10] mounted on a ceramic ("alsimag") slab. The YIG squares are placed opposite the gaps between the fingers, where the polarization is most circular. The spacing of the strip of isolators from the fingers is most critical in determining the maximum ratio of reverse to forward loss. The shape of the YIG pieces is not ideal from the point of view of linewidth, but it is much easier to fabricate an isolator strip of this form than ellipsoids. Tuning the broad resonance of the isolator to the ruby line is accomplished by controlling the YIG thickness, which in this case is about .004 .

The presence of the isolators is very essential to the operation of the maser on account of the impossibility of producing a really satisfactory match between the comb structure and the external coaxial line. The fundamental difficulties are due to the fact that the propagation constant along the comb varies by about two orders of magnitude across the passband, and furthermore, the coupling between the resonant elements (fingers) is by no means limited

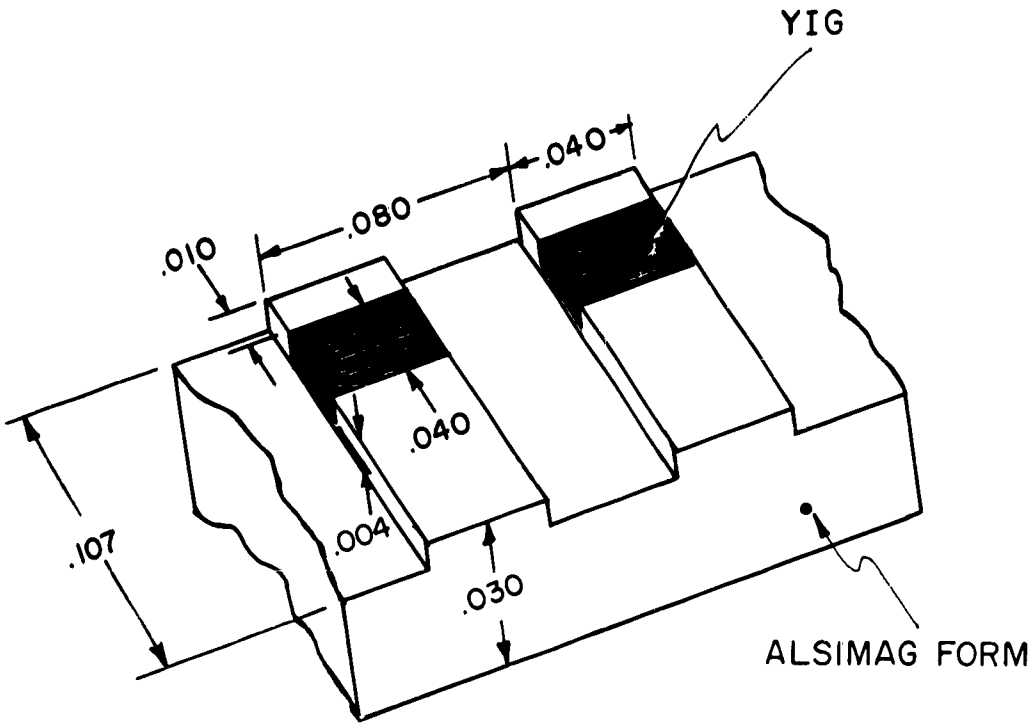

FIG. 4 SECTION OF ISOLATOR STRIP

to nearest neighbors. This makes it impossible to match the structure by a single element [11]. The reflections at the probes would cause oscillation were it not for the isolator. The minimum isolation needed, however, is not that required to prevent oscillation, because the feedback will cause rapid variations in transmitted power as a function of frequency. Extra isolation must be provided to smooth the gain-versus-frequency curve at constant magnetic field. For this reason we use two isolator strips of the type shown in Fig. 4, one mounted on top of the other.

In designing a TWM one must decide the tunable bandwidth and gain required. The tunable bandwidth must necessarily be limited to the passband of the structure, and is usually only about 75 % of this because of forward loss in the isolator and increased structure losses near the ends of the band. The bandwidth, of course, limits the available slowing factor.

Fig. 2 illustrates a typical geometry used in loading the comb with dielectric. The presence of alumina, whose dielectric constant is close to that of the single crystal ruby (about 9), is determined only by the quantity of ruby available. Usually, no more than about 10 % filling factor is lost in the design by using alumina instead of ruby, and this accounts for about 3 dB loss in gain.

The most difficult problem (apart from construction of the comb) is in constructing a loaded structure having the desired passband (to provide

the required tuning range) and satisfactory dispersion characteristics. These properties are most conveniently studied by using a structure having the same design as the comb but of shorter length. For this purpose a sixteen-element comb was used.

The type of information obtained from the small comb is illustrated in Figs. 5 and 6. These figures are plots of reflection coefficient as a function of frequency obtained with a small probe located at the end of the structure, which couples weakly into the structure. The sixteen-element structure is a sixteen-mode oscillator in which the phase difference between the end elements can have the values $0, \pi, 2\pi, \ldots 15\pi$. Measurement of these resonant frequencies gives the ω-β relation directly, and these curves are plotted directly below the reflection coefficient curves. With insufficient coupling, fewer than sixteen resonances will be seen. This is the case in Fig. 6.

Figure 5 shows the characteristics for a comb loaded with alumina only, while Fig. 6 shows the effect of increased dielectric loading in the form of rutile strips of .010 x .050 cross section near the tips of the fingers. The increased effect of the rutile with increasing frequency can be easily understood when one notes that (i) the rf electric fields are strongest near the finger tips; (ii) the rf fields become more concentrated toward the fingers as the propagation constant increases; (iii) the dielectric constant of polycrystalline rutile is high (about 100); and (iv) ω is an increasing function of β

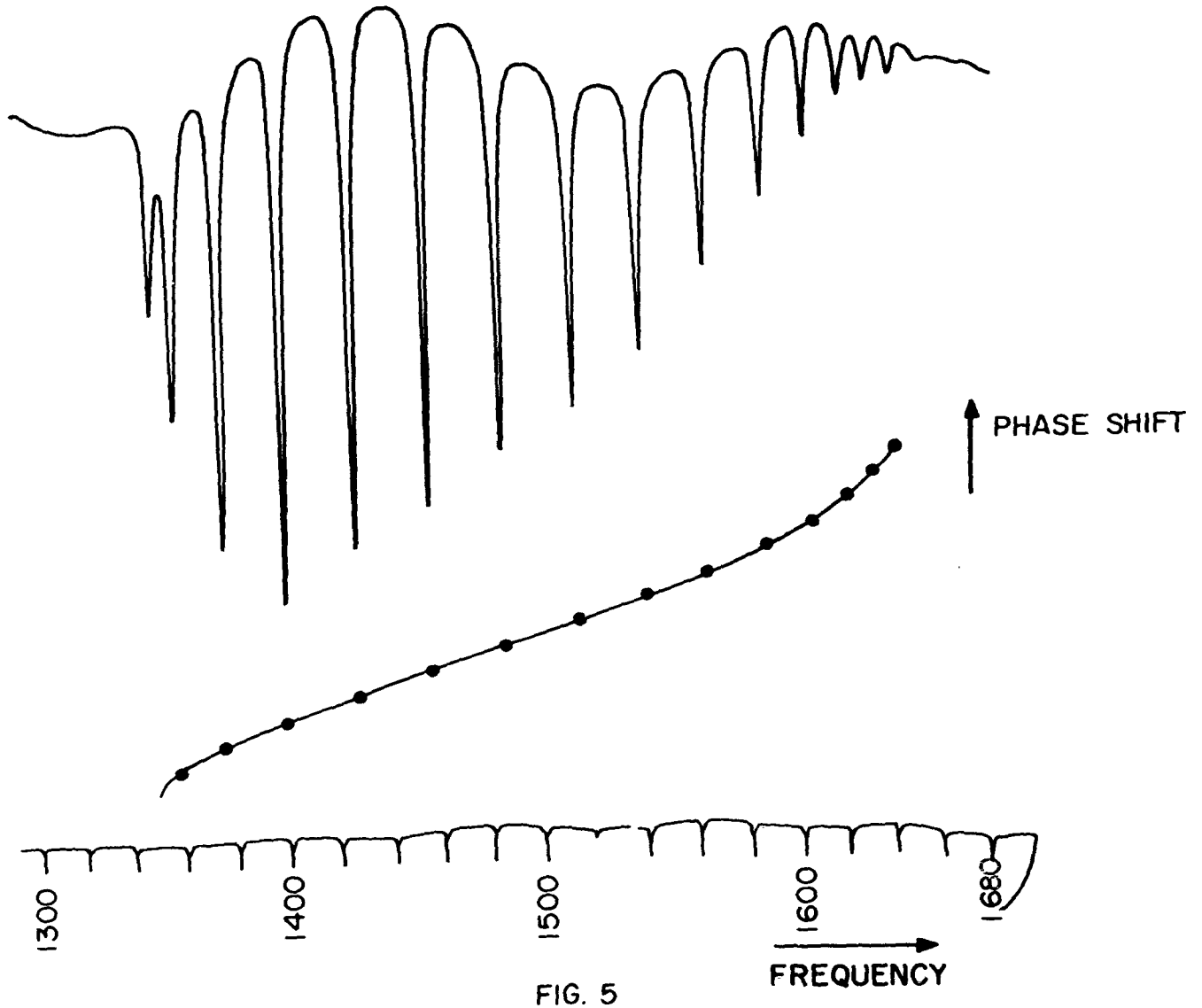

FIG. 5

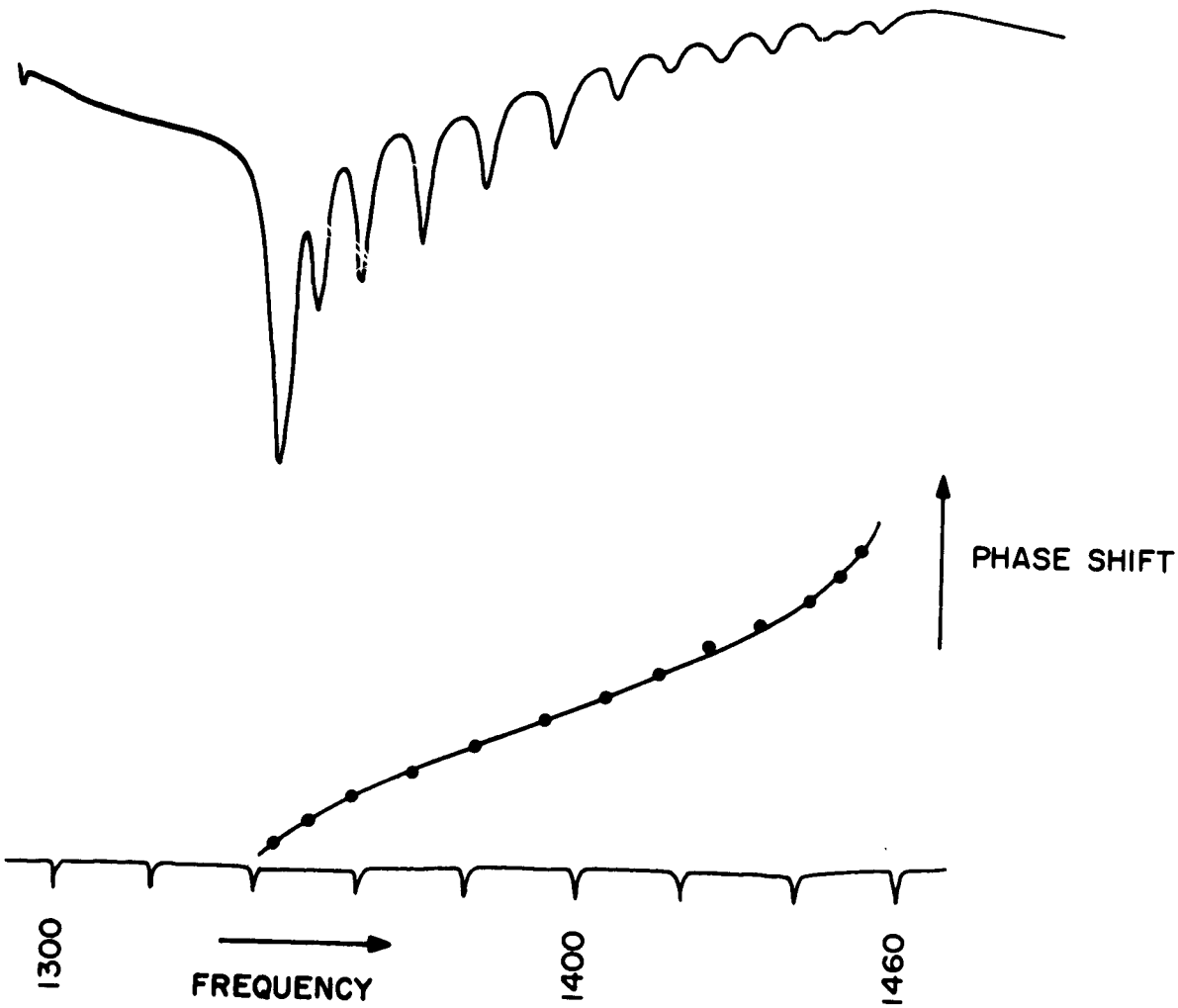

FIG. 6

in this structure. On the basis of the information obtained from many such measurements using different loading geometries, the influence of various changes in the loading configuration on the details of the ω -β relation can be deduced.

At the lower cut-off frequency, the electric field lines run between the fingers and walls, not between fingers, so that this frequency is determined mainly by the height of ruby and alumina and its thickness. This frequency can be controlled by adjusting the ruby thickness without affecting the upper cut-off frequency, and is most sensitive to removal of material in the region of strong electric field. A bevel can be ground into the alumina as shown in Fig. 2 to raise the lower cut-off frequency.

Determination of the upper and lower cut-off frequencies is not sufficient in the design of a TWM . One can trim the dielectric in such a way that for a given frequency ω, the propagation constant β along the comb will be double-valued. The two values of β correspond to different field configurations, one a forward wave, the other backward. The backward wave will be amplified in spite of the isolator, since its sense of polarization is determined by the phase propagation. This condition causes oscillation. The multiple-valued ω-β relation is well known in other periodic structures [11], and is caused by excessive coupling between non-adjacent elements. With a given comb configuration, dielectric loading will narrow the passband to a certain minimum value, after which further shaping of the dielectric in an attempt

to narrow the band further will cause the double-valued ω-β characteristic. The cross-section dimensions of the rutile, of the bevel in the alumina, and the thickness of the air gap between the ruby and side walls have been chosen to produce a structure in which ω is an increasing function of β.

The best way to reduce the coupling between non-adjacent elements of the comb is to reduce the width of the housing. This has been done in the present design in which the inside dimensions are .260 x .900 whereas normal X-band waveguide has the dimensions .400 x .900. The maximum slowing factor in the center of the passband is about 420 using the narrow structure, compared to about 280 with the standard X-band housing. In narrowing the passband one obtains increased gain at the expense of tuning range.

IV. Effects of Mechanical Imperfections

The details of the ω-β relation can be changed drastically by mechanical imperfections in the structure. The effects are particularly serious here compared to earlier TWM's because of the heavy dielectric loading. The most important imperfections are:

(a) Variation in finger-to-finger spacing

(b) Misalignment of fingers

(c) Variation in finger cross-section dimension

(d) Variation in cross-section dimensions of dielectric materials.

Effects (a), (b), and (c) will change the finger-to-finger "capacitance", and this effect shows up principally in the higher-frequency part of the passband where the electric flux tends to be directed along the comb more than to the side walls. Internal reflections result, and the reflected power is lost into the isolator. The gain-versus-frequency curve then shows fluctuations that become larger as the frequency approaches the upper cut-off, together with a steady decrease in gain with increasing frequency. Effect (b) can be partly compensated by increasing the pressure on the fingers from the dielectric. The presence of rutile enhances the effects of the imperfections since it magnifies the irregularity in electrical coupling between the fingers.

The upper cut-off frequency is strongly perturbed by the imperfections. Different comb structures with the same dielectric loading may show variations of about 20 Mc in this frequency. Similarly, the lower cut-off frequency is very sensitive to the thickness of the gap between the dielectric and side walls. A change of .001 in this dimension on both sides of the comb will change this frequency by about 20 Mc . A taper in this dimension will, therefore, adversely affect the low-frequency part of the ω-β relation.

In view of the seriousness of tapers and mechanical irregularities, all the dielectric materials have to be accurately ground, and exceptional precision is required in the fabrication of the comb. Furthermore, great pains are taken to ensure the intimate contact of the dielectric with the comb surfaces.

The most serious of the imperfections is the variation in finger-to-finger spacing. Unfortunately, this imperfection can be induced in a perfect maser structure by the thermal cycling between helium and ambient temperatures as a result of the difference in thermal expansion coefficients between the copper and the ruby etc. It was found that the forward losses in the maser increased progressively with each test owing to this phenomenon, the effect being worse at higher frequencies, and almost unnoticeable near the lower cut-off frequency.

The effect of the thermal cycling on the periodicity can be counteracted by use of a finger-spacer. This consists of a long thin alumina strip with teeth ground into one edge with a periodicity of .080 . The spacer is mounted on top of one side of the dielectric loading and mates into the top part of the comb when the loading is pressed against the comb. (See Fig. 7) In this way the comb is held rigidly and should stay that way indefinitely.

V. The Magnet

Since the magnetic field has to be applied in the direction shown in Fig. 1, long rectangular poles have to be used. The field is provided by a permanent magnet with rectangular pole pieces 8 x 3 spaced 2.3 inches apart. The magnet design is based on that used for the masers in "Project Echo", which is due to P. Cioffi (unpublished). A large fraction of the Alnico V yokes was removed since the operating field is now 2000 gauss instead of 2530 gauss.

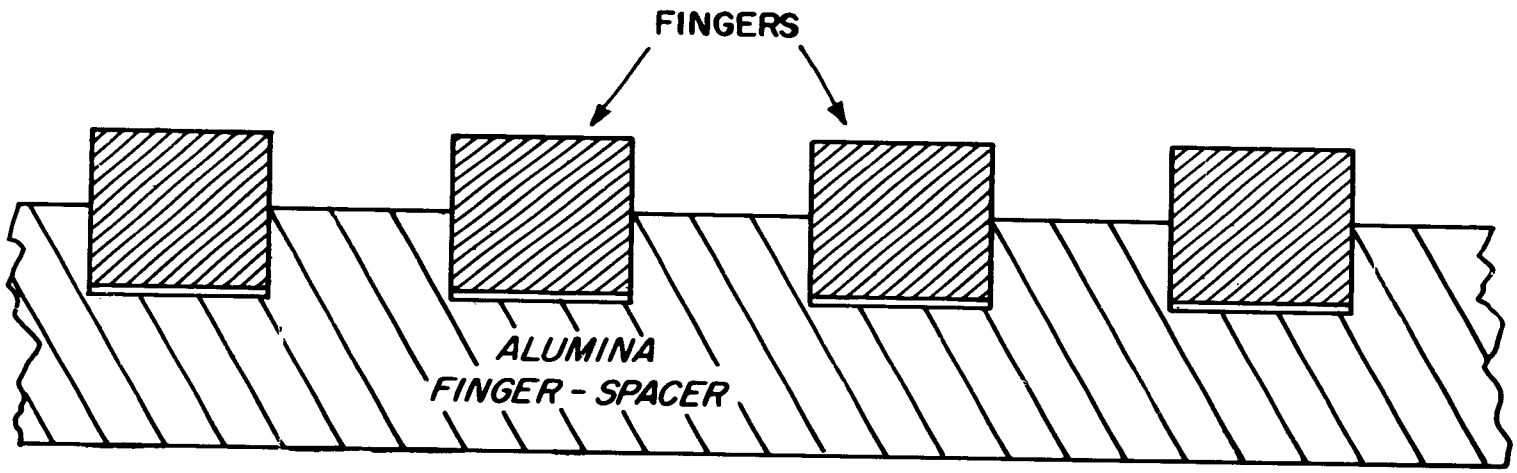

FIG. 7 THE FINGER-SPACER

Although the magnet was designed to give a field of 2400 gauss with the Alnico V magnetized to saturation, an improved method of charging the magnet caused a saturation field of 2930 gauss. On demagnetizing to 2000 gauss the magnet thus exhibits high stability. The field is tunable from 1920 gauss to 2035 gauss by means of movable shunts. The field is reproduced as the shunts are cycled owing to the high saturation field obtainable. (A less stable magnet, i.e., one whose operating field is closer to the saturation value, would gradually demagnetize as the shunts are cycled.)

The weight of the magnet is 230 lb. and the field is homogeneous to within 0.1 % (2 gauss) over the volume of the ruby in the maser. Shims are used on all four edges of each pole to provide this homogeneity.

A photograph of the magnet is shown in Fig. 8. The shunt mechanisms are clearly visible in the picture. The two worms on the shunt drives are driven in synchronism to move the shunts symmetrically.

VI. The Dewar

The stainless steel Dewar was built by Hofman Laboratories, Inc. It stores 7 liters of helium and 14.5 liters of nitrogen. It can be tilted to an angle of 50° from the vertical. The tail section has an inside diameter of 1.7 inches and outside diameter of 2.220 . The Dewar tail fits between the poles of the magnet.

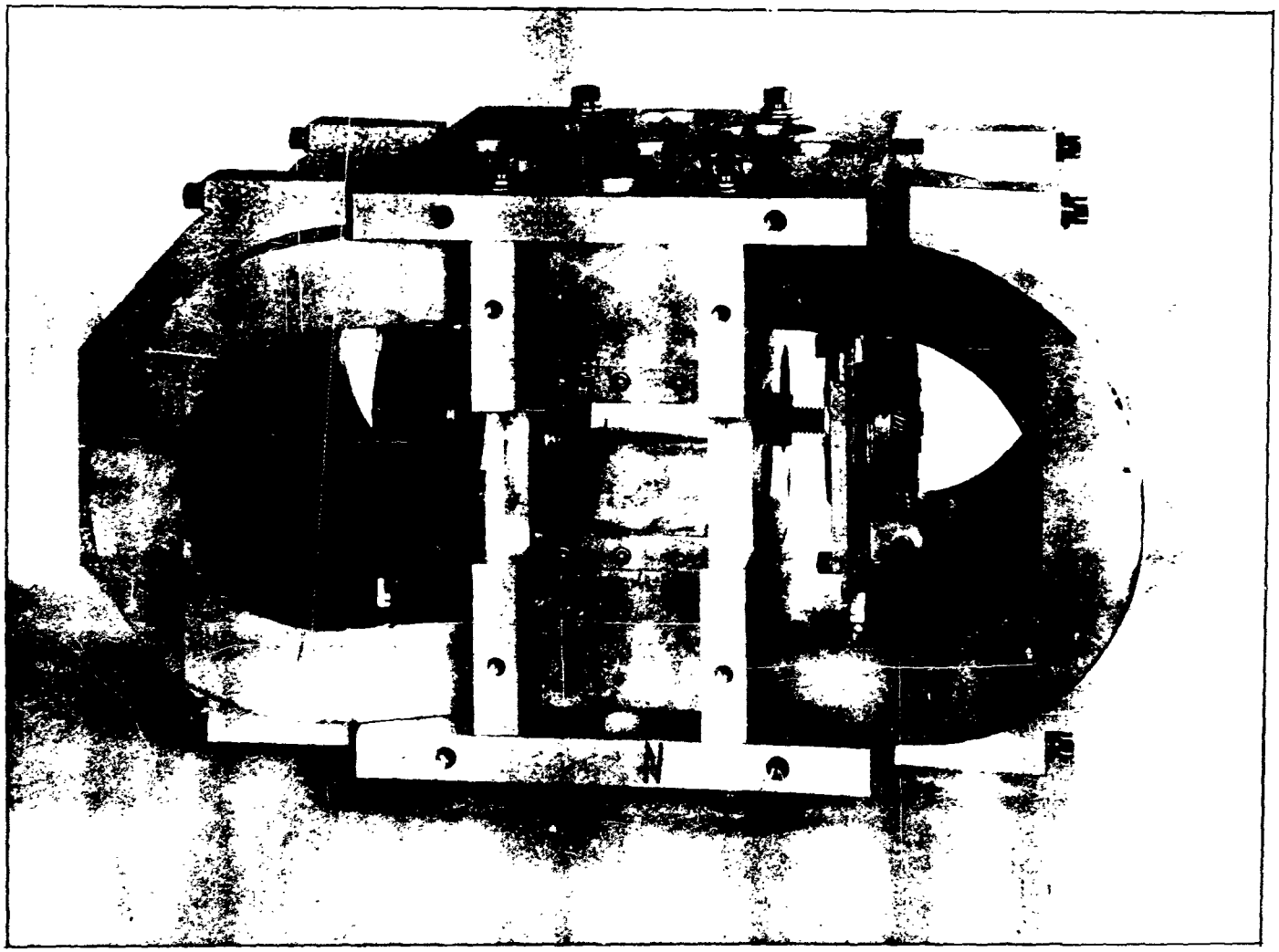

FIG. 8 THE MAGNET

VII. Characteristics of Maser

A. Inversion Ratio

One of the most important measurements made in connection with maser performance is that of inversion of the populations n_1 and n_2 of the lower and upper levels of the signal transition under the action of the pump. The inversion ratio I is defined by the relation

$$(n_2 - n_1)_{\text{pumped}} = I\,(n_1 - n_2)_{\text{thermal}}$$

The product $I\,(n_1 - n_2)_{\text{thermal}}$ which is proportional to I x concentration of Cr^{+++} ions is the important quantity, and at L-band is maximum for a molar concentration of Cr_2O_3 in the Al_2O_3 of about .04 %. The inversion ratio I is a function of temperature and concentration and its value depends on the details of the relaxation processes. A measurement of I at 4.2°K gives an indication of the ruby concentration, and is a powerful method of detecting strains in the ruby crystal. For example, if the slowing factor is right, the inversion ratio suitable, and the maser gain is too low, we know that the filling factor is too small, this usually being caused by twinning in the ruby crystal. This enables one to correlate the appearance of a ruby crystal between crossed polaroids with performance in the maser.

The inversion ratio is measured in the following way. One notes the difference in dB of input signals required to produce the same output with pump on and pump off.

This gives a reading proportional to

$$\chi''_{thermal} - \chi''_{pumped} .$$

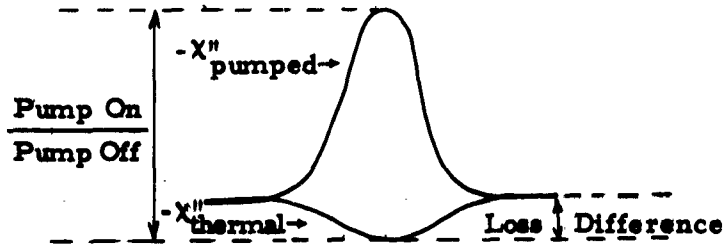

Next one measures the dB difference in loss through the structure at low signal level and high signal level (where the signal transition is saturated), the pump being turned off. This gives a reading proportional to $\chi''_{thermal}$. An alternative method of obtaining the latter number is to compare the loss at resonant absorption to that with the field detuned off the ruby resonance but still on the broad isolator resonance. The two methods give consistent results. From the two measurements one obtains the ratio I. The numerical example below is typical of the results obtained. The input power required to give the same output under three different conditions is:

Pump On - 90 dBm

Pump Off - 53 dBm

Field Detuned - 58 dBm

Therefore,

$$I = \frac{90 - 58}{58 - 53} = 6.4$$

B. Gain measurements

The gain formula, shown in Eq. 6, gives the "electronic gain", from which one must subtract the structure and isolator losses to obtain the net gain. The net gain is measured directly, and at the same time one measures the power change in dB to produce the same output power with pump on and pump off, respectively. Knowing the value of I, one computes the electronic gain from this latter measurement.

The results of a set of such measurements are presented in Table I. These results apply to a maser unit about six inches long containing 72 fingers. In computing the electronic gain from the Pump On ÷ Pump Off measurements an inversion ratio of 6.4 was assumed. The losses are computed by subtracting the second column entries from the fourth column. At each frequency listed the magnetic field and pump frequency have been adjusted to optimum values. The entries in the table thus give the tuning characteristics, not the instantaneous gain-bandwidth relation. The instantaneous 3 dB bandwidth is 15 Mc, which is consistent with a 45 Mc half-width Lorentzian χ'' for the L-band transition. This indicates a uniform inversion of the transition.

Notice that the forward loss in the structure increases towards the two ends of the band. This is a result of the greater slowing factor there, as well as the approach to linear polarization, this causing an increased forward loss in the isolator.

Table I - Gain Characteristics of Single Maser Unit at 4.2°K.

Frequency	Net Gain	$\frac{\text{Pump On}}{\text{Pump Off}}$	Electronic Gain	Structure Loss
1320 Mc	12 dB	29 dB	25 dB	13 dB
1330	14	29	25	11
1340	18	29.5	25.5	7.5
1350	19	29.5	25.5	6.5
1360	20	31	27	7
1370	20.5	31	27	6.5
1380	20	32.5	28	8
1390	20	33	28.5	8.5
1400	20.5	35	30	9.5
1410	20.5	37	32	11.5
1420	20.5	39.5	34	13.5
1430	19.5	41.5	36	16.5
1440	19	46	40	21

Lower Cut-Off Frequency = 1290 Mc

Upper Cut-Off Frequency = 1465 Mc

A 20 dB gain with 15 Mc instantaneous bandwidth is quite good, but not ideal. A second stage amplifier that has an input noise temperature of 1200°K would contribute 12°K to the equivalent input temperature of the preamplifier. This is really not tolerable if one is aiming at an overall input temperature of 50°K .

Figure 9 is a photograph of the two maser units joined in series, while Fig. 10 shows the maser connected to its head assembly. The X-band waveguide carries the pump power to a power divider which feeds the two units. A gain of 26 dB would reduce the second stage noise contribution to the tolerable level of 3°K. To obtain the higher gain, two maser units have been built and connected in series. The gain of the second unit measures consistently 2 or 3 dB lower than that of the first unit, for which the results are shown in Table I . In a homogeneous magnetic field the total net gain of the two units is about 37 dB, with an instantaneous bandwidth of about 11 Mc. By appropriately shimming the magnet, gain can be efficiently traded for bandwidth.

The inhomogeneity of the magnet used with this maser is such that the net gain of the two units is 33 dB and the instantaneous bandwidth about 11 Mc. (See Table II). An uncontrolled inhomogeneity, (in this case caused by removal of material from the magnet shims to allow the dewar to fit) is not an efficient mechanism for broadening the response of the amplifier. The reason for this is that the gain in dB is proportional to X'', and an increase in the

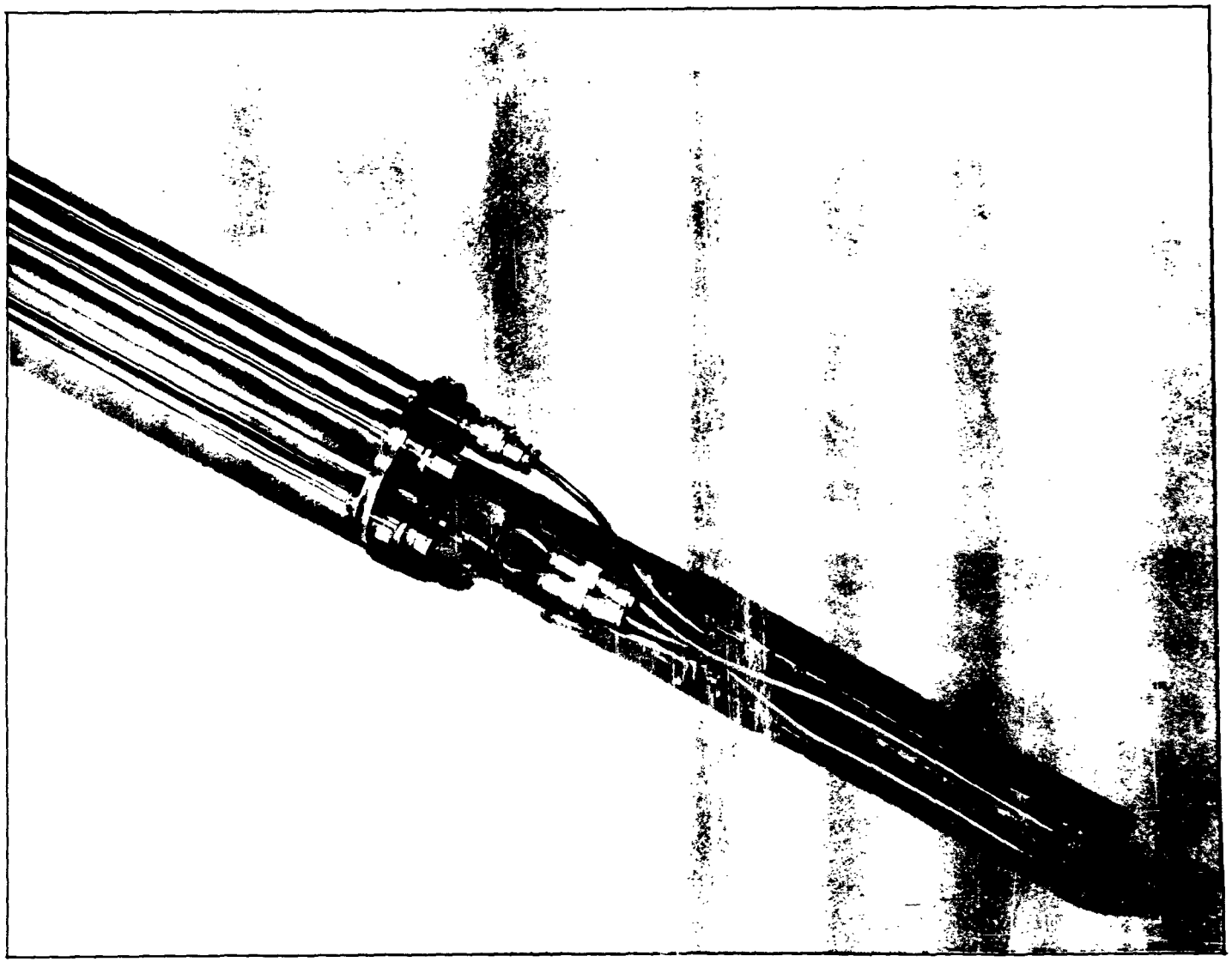

FIG. 9 MASER UNITS JOINED IN SERIES.

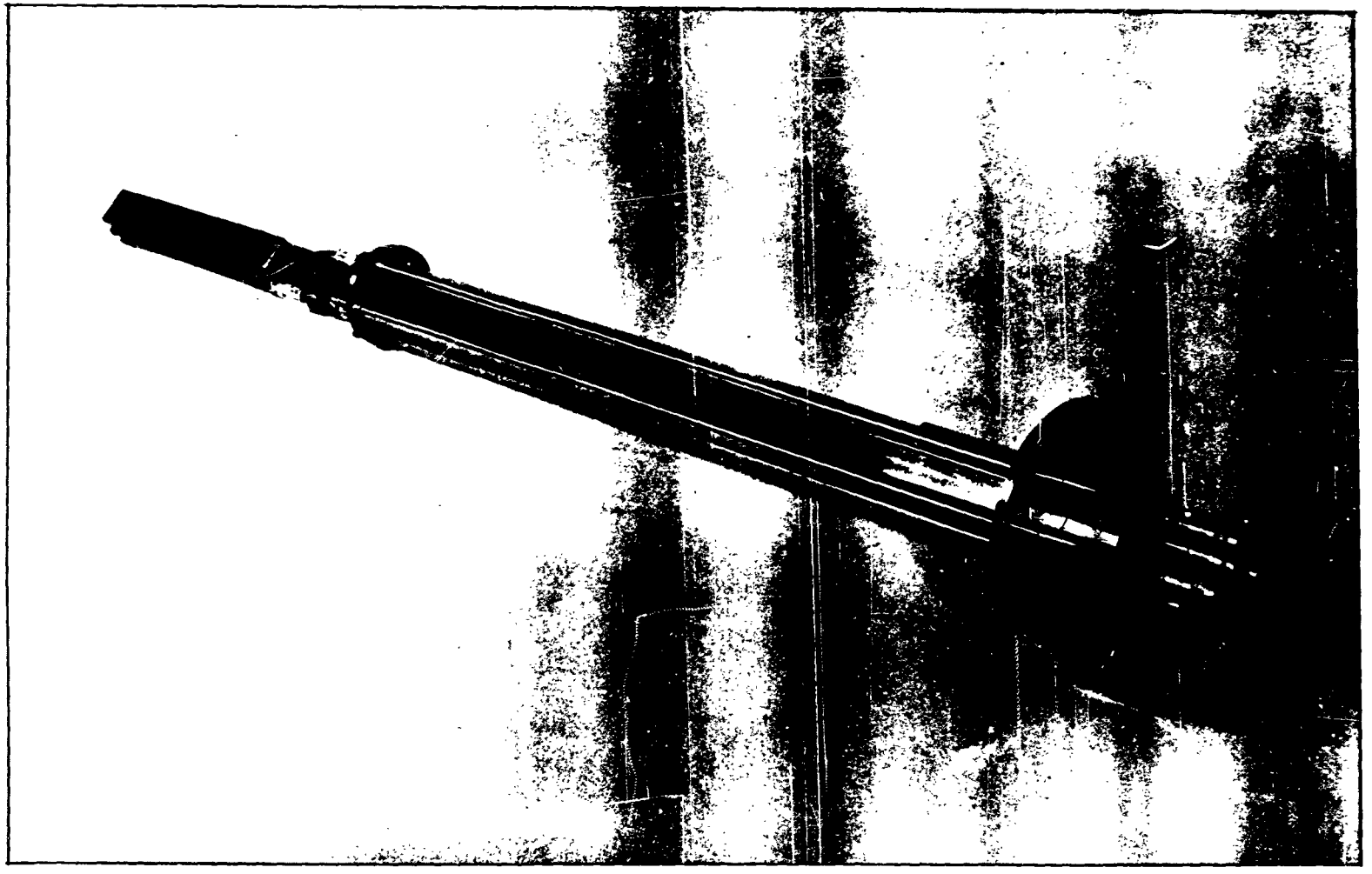

FIG. 10 MASERS JOINED TO HEAD ASSEMBLY.

X" half-width does not necessarily imply a broadening between the 3 dB points of the gain-frequency characteristic. By producing a step of approximately five gauss in the magnetic field, the bandwidth can be increased to 15 Mc with a loss in gain of less than 7 dB.

C. Saturation

When the input signal becomes too strong, the L-band transition starts to saturate, first in the ruby near the output end of the maser, then the region of saturation moves down the maser towards the input end as the power is increased. Measurements show that the saturation sets in very gradually, and becomes noticeable (i.e., with a 1 dB loss in gain) when the output power is about - 40 dBm. Saturation in the input signal is not important in radio astronomy. What is important, however, is the fact that the maser can be saturated by leakage of the local oscillator power from the following crystal mixer back into the maser. The fact that the local oscillator is tuned 30 Mc away does not matter very much because the transverse relaxation mechanism in the spin system is very effective. For this reason it is desirable to use a 60 Mc i. f. and put a 20 dB isolator following the output of the maser.

Table II - Gain Characteristics of Double Maser System

Frequency	Net Gain
1430 Mc	26 dB
1420	33
1410	34
1400	33
1390	33
1380	32.5
1370	34
1360	32
1350	30
1340	29
1330	20

VIII. Anticipated Performance

The radiometer system using the maser as preamplifier will be operated as a Dicke switch. It is expected that the overall system temperature will be less than $50^{\circ}K$ as indicated in the estimate below.

Antenna Spillover plus Input Cable Losses	$< 30^{\circ}$
Circulator Switch	10°
Maser	4°
Second Stage	3°

The present radiometer system, using the cavity maser , has a total system temperature of $100 \pm 10^{\circ}K$.

The radio astronomers will be able to make good use of the TWM . The large bandwidth can be used for studying clusters of galaxies, or alternatively, for searching a very large depth of the sky for individual galaxies. Furthermore, for observation of continuum radiation, the sensitivity is proportional to $\sqrt{B\tau}$ where B is the instantaneous bandwidth, and τ the time constant of the final filter. If we assume

$$B = 10 \text{ Mc} = 10^7 \text{ sec}^{-1}$$

and

$$\tau = 10 \text{ sec}$$

and use the formula $\Delta T = \dfrac{T_o}{\sqrt{B\tau}}$ where ΔT is the smallest detectable antenna input temperature change and T_o is the input system temperature, we obtain

$$\Delta T = 5 \times 10^{-3} \ ^{o}K \ .$$

The extent to which such an estimate must be raised on account of gain fluctuations in the maser and residual unbalance of the antenna temperature with the reference noise source will be known at some later date, but no difficulty is anticipated. The TWM is basically a much more stable amplifier than the cavity maser. In fact, measurements made at Bell Telephone Laboratories have failed to detect any gain fluctuations.

An important feature of the design is the tuning range, which goes down to 1340 Mc, corresponding to a Doppler shift of 80 Mc in the hydrogen line. This corresponds to a distance of almost 100 Mpc or 3.7×10^{8} light years. Study of hydrogen radiation with instruments such as the TWM described here, in conjunction with good antennas, is bound to yield very valuable information on the structure of the universe.

Acknowledgments

The author spent nine months at Bell Telephone Laboratories, Murray Hill, New Jersey, as a Resident Visitor during the time of the actual development and construction of the maser. During this period the cooperation of Mr. M. L. Hensel was most valuable, as was consultation with other members of the (Bell Telephone Laboratories) technical staff, in particular Dr. H. E. D. Scovil and Dr. E. O. Schulz-DuBois. Bell Telephone Laboratories made all the parts of the maser and the head assembly for it, and also provided some of the parts for the magnet. The magnet was charged by Mr. E. Mc Dermott at BTL Magnet Laboratory. The interest and encouragement given by Prof. N. Bloembergen and Prof. A. E. Lilley are greatly appreciated.

This research has been supported by the Office of Naval Research and the National Science Foundation.

References

1. Oort, J. H. , "Radio Frequency Studies of Galactic Structure", Encyclopedia of Physics, Vol. 53, (Springer-verlag) p. 100, 1959.

2. The megaparsic (Mpc) is the distance at which a sphere with a diameter equal to that of the earth's orbit about the sun would have an angular size of 10^{-6} second of arc. One parsec equals 3.7 light years.

3. Bloembergen, N., "Proposal for a New-Type Solid State Maser", Phys. Rev. 104, p. 324 , October, 1956.

4. Jelley, J. V., and Cooper, B. F. C., Rev. Sci. Instr. 32, 166 .

5. Epstein, E. E., "Atomic Hydrogen in Galaxies", Ph. D. Thesis, Harvard University, Department of Astronomy, April, 1962.

6. Schulz-Du Bois, E. O., "Paramagnetic Spectra of Substituted Sapphires - Part I : Ruby", Bell System Tech. J. 38, p. 271 , January, 1959.

7. Weber, J., Revs. Mod. Phys. 31, 681, 1959 .

8. De Grasse, R. W., Schulz-Du Bois, E. O., and Scovil, H. E. D., " The Three-Level Solid State Traveling-Wave Maser", Bell System Tech. J. 38, p. 1, March, 1959 .

9. De Grasse, R. W., Kostelnick, J. J., and Scovil, H. E. D., "The Dual Channel 2390 Mc Traveling-Wave Maser", Bell System Tech. J. 40, p. 1117, July, 1961.

10. All dimensions in this paper are in inches, unless otherwise stated.

11. Brillouin, L., "Wave Propagation in Periodic Structures", Dover Publications, New York , 1953 .

Armitry Supply Officer
Building 1310, Charles Wood Area
Fort Monmouth, New Jersey (10)
Attn: Director of Research

Commanding Officer
Office of Naval Research
Navy 100, Box 39 (25)
Fleet Post Office
New York, New York

Armed Services
Technical Information Agency
Arlington Hall Station (10)
Arlington 12, Virginia
Attn: TIPDR

The Director
Naval Research Laboratory
Washington 25, D. C (6)
Attn: Technical Information Officer

Commanding, AF CRL
LFSD, AFCRC, CRELG
Laurence G. Hanscom Field (6)
Bedford, Massachusetts
Attn: Electronics Research Directorate

Commanding General
Air Research and Development Command
P. O. Box 1395 (2)
Baltimore 3, Maryland
Attn: RDTAR

Chief of Naval Research
Department of the Navy (2)
Washington 25, D. C.
Attn: Dr. A. Shostak, Code 427

Chief of Naval Research
Department of the Navy (2)
Washington 25, D. C.
Attn: Code 427

Commanding Officer
Office of Naval Research
495 Summer Street (2)
Boston, Massachusetts

Chief, Bureau of Ships
Department of the Navy (2)
Washington 25, D. C.
Attn: Code 810

Director, Air University
Library (2)
Maxwell Air Force Base
Alabama

Chief of Naval Research
Department of the Navy
Washington 25, D C
Attn: Code 421

Commanding Officer
Office of Naval Research
495 Summer Street
Boston, Massachusetts

Commanding Officer
Office of Naval Research
John Crerar Library Building
86 East Randolph Street
Chicago 1, Illinois

Commanding Officer
Office of Naval Research
346 Broadway
New York 13, New York

Commanding Officer
Office of Naval Research
1030 East Green Street
Pasadena, California

Commanding Officer
Office of Naval Research
1000 Geary Street
San Francisco 9, California

Head, Document Section
Technical Information Division
Naval Research Laboratory
Washington 25, D C

Martin A. Caroiano
Magnetism Branch, Code 6456
Solid State Division
Naval Research Laboratory
Washington 25, D. C

Commanding Officer
U S. Air Development Center
Johnsville, Pennsylvania
Attn: NADC Library

Commander
U S. Air Development Center
Johnsville, Pennsylvania
Attn: AASL

Chief, Bureau of Aeronautics
Department of the Navy
Washington 25, D C
Attn: RS-1

Engineering Librarian
Convair
San Diego 12, California

Dr. John B. Pippin
Applied Physics and Ferrite Devices
Sperry Microwave Electronics Co.
P. O. Box 1828
Clearwater, Florida

Engineering Library
Sperry Microwave Electronics Co.
Clearwater, Florida

Dr. Lajos Rimai
Research Division
Raytheon Company
Waltham 54, Massachusetts

Elizabeth Weeks, Librarian
Raytheon Company
30 Hyrne Street
Waltham 54, Massachusetts

Report Librarian
Sylvania Electric Products Inc
Electronic Systems Division
100 First Avenue
Waltham, Massachusetts

Document Control Center
Wayland Laboratory
Raytheon Manufacturing Co
Wayland, Massachusetts

J. B. Goldman
Scientific Laboratory
Ford Motor Company
Engineering Staff
P. O. Box 2053
Dearborn, Michigan

Charles C. H. Tung
Bell Telephone Labs.
Murray Hill, New Jersey

Librarian
RCA Laboratories
Princeton, New Jersey

Dr. A. Ament
RCA
Princeton, New Jersey

Commander (2)
U. S. Naval Electronics Lab
San Diego, California

Commanding General, RCRW
Rome Air Development Center
Griffiss Air Force Base (2)
Rome, New York

Commanding General
Air Research and Development Command
P. O. Box 1395 (2)
Baltimore, Maryland
Attn: RDSRS

Commander
Air Force Cambridge Research Labs.
Laurence G. Hanscom Field (2)
Bedford, Massachusetts
Attn: CROTLR

Commander
Wright Air Development Center
Wright Patterson Air Force Base (2)
Ohio
Attn: WCLRA Library

National Security Agency
Physical Sciences Division (2)
Fort George Meade, Maryland
Attn: Dr. Edwin Meckler

Associate Prof. A. Moretellan
Department of Electrical Engineering
University of Southern California
University Park
Los Angeles 7, California

Assistant Secretary of Defense
(Research and Development)
Research and Development Board
Department of Defense
Washington 25, D. C

Chief of Naval Operations
Department of the Navy
Washington 25, D. C.
Attn: Op-20

Chief of Naval Operations
Department of the Navy
Washington 25, D. C
Attn: Op-32

Chief of Naval Operations
Department of the Navy
Washington 25, D. C
Attn: Op-413

Chief, Bureau of Aeronautics
Department of the Navy
Washington 25, D C
Attn: EL-4

Technical Library
U S Naval Proving Ground
Dahlgren, Virginia

Director
Naval Ordnance Laboratory
White Oak, Maryland

Librarian
U S Naval Post Graduate School
Monterey, California

Air Force Office of Scientific Research
Air Research and Development Command
Washington 25, D C
Attn: SRY, Physics Division

Commanding General
Rome Air Development Center
Griffiss Air Force Base
Rome, New York
Attn: RCRRC-GC

Commanding General
Rome Air Development Center
Griffiss Air Force Base
Rome, New York
Attn RCR

Commander
Air Force Cambridge Research Center
730 Albany Street
Cambridge 39, Massachusetts
Attn: CRRI

Commander
Air Force Cambridge Research Center
130 Albany Street
Cambridge 39, Massachusetts
Attn. CRRM

Commander
AF Cambridge Research Laboratories
Laurence G. Hanscom Field
Bedford, Massachusetts
Attn: Dr Hollingsworth

Commander
Wright Air Development Center
Wright Patterson Air Force Base
Ohio Attn: WCRR

Sandia Corporation
Org 1636, Sandia Base
Albuquerque, New Mexico
Attn: Dr. C W Harrison, Jr

Sandia Corporation
Sandia Base
Albuquerque, New Mexico
Attn: Library Division 1932-1

Mr Robert Turner
General Electric Company
Advanced Electronics Center
Cornell University
Ithaca, New York

Library
Airborne Instruments Lab
Walt Whitman Road
Melville, Long Island New York

Secretary, Working Group
Semiconductor Devices
366 Broadway, 8th Floor
New York 13, New York
Attn: AGRT

Metals Research Laboratories
Electro Metallurgical Company
Box 586, Niagara Falls New York
Attn: Mr. R. J Gladieux

Librarian
General Electric Research Lab.
P O Box 1088
Schenectady, New York

Westinghouse Electric Corp
Research Laboratories
Beulah Road, Churchill Boro
Pittsburgh 35, Pennsylvania

Prof. O. E. H. Rydbeck
P. O. Box 246
Bolmar, New Jersey

Dr. Melvin W Aarons
611 East Genesseo Street
Fayetteville, New York

Laboratory
Airborne Instruments
Mineola, New York

Commander
Wright Air Development Center
Wright Patterson Air Force Base
Ohio
Attn: WCRRH

Commandant
Air Force Institute of Technology
Wright Patterson Air Force Base
Ohio
Attn: MCLi Library

AF Special Weapons Center
Kirtland Air Force Base
Albuquerque, New Mexico
Attn: SWOI

Headquarters
AF Missile Test Center
MU-135, ARDC
Patrick Air Force Base
Florida

U S. Coast Guard
1300 E Street, N W.
Washington 25, D C
Attn: EER

M. A. Kriswasish, Chief
Systems Components Branch
Electronic Warfare Division
Signal Corps Agency
White Sands Proving Ground
New Mexico

Mr. A. D Bedrosian
Signal Corps Liaison Office
Mass. Institute of Technology
Building 26, Room 131
Cambridge 39, Massachusetts

Chief, European Office
ARDC Command
Mail Building
60 Rue Ravenstein
Brussels, Belgium

Dr J. Amos Hofman
Ordnance Materials Res. Office
Watertown Arsenal
Watertown, Massachusetts

Acquisitions Officer
ASTIA Reference Center
Arlington Hall Station
Arlington 12, Virginia

Stanford Research Institute
Documents Center
Menlo Park, California
Attn: Mary Lou Fields

Dr C M Pepas
Dept of Electrical Engineering
California Institute of Technology
Pasadena, California

Stanford Electronics Lab
Stanford University
Stanford, California
Attn Document Library
Applied Electronics Lab

Department of Electrical Engineering
Yale University
New Haven, Connecticut

Librarian
Johns Hopkins University
1315 St Paul Street
Baltimore 2, Maryland

Radiation Laboratory
Johns Hopkins University
1315 St Paul Street
Baltimore 2, Maryland

Director, Lincoln Laboratory
Mass Institute of Technology
Bedford, Massachusetts

Mr John Hewett
Document Room
Research Lab of Electronics
Mass Institute of Technology
Cambridge 39 Massachusetts

Professor A Von Hippel
Mass Institute of Technology
Lab for Insulation Research
Cambridge 39 Massachusetts

Library, Room A 229
Lincoln Laboratory
P O Box 73
Lexington 73 Massachusetts

K M Siegel, Head
Theory and Analysis Department
Willow Run Laboratories
University of Michigan
Willow Run Airport
Ypsilanti, Michigan

Librarian
National Bureau of Standards Library
Room 301, Northwest Building
Washington 25, D C

Librarian
U. S. Department of Commerce
National Bureau of Standards
Boulder, Colorado

Dr Earl Callen
National Security Agency
Physical Sciences Division
Fort George Meade, Maryland

Dr N Campagna
National Security Agency
Physical Sciences Division
Fort George Meade, Maryland

Chung Kung University
Electrical Engineering Department
Taipei, Taiwan
Republic of China
Attn: Professor Chao-Mei Chiu
Head, Eng. Department

Mr D S. Jones
Department of Mathematics
Univ. College of Nn. Staffordshire
Keele, Staffordshire, England

Professor Paul Sumi Mao
Chung Hsing University
Dept. of Engineering Sciences
12 Nishi Ogimachi Kimita
Osaka, Japan

Donald C. Stinson
Dept. of Electrical Engr.
University of Arizona
Tucson 25, Arizona

Professor Jerome R Singer
Div. of Electrical Engineering
University of California
Berkeley 4, California

Professor Charles Kittel
Department of Physics
University of California
Berkeley 4, California

Bartels Library
Brandeis University
Waltham, Massachusetts

Professor N G Roeder
School of Electrical Engineering
Cornell University
Ithaca, New York

Library, College of Engineering
University Heights Library
University Heights
New York University
New York 53, New York

E A Chapman, Librarian
Rensselaer Polytechnic Institute
Amos Eaton Hall
Troy, New York

Robert Pinnoy
Department of Engineering
Case Institute of Technology
University Circle
Cleveland 6, Ohio

Dept. of Electrical Engineering
Case Institute of Technology
University Circle
Cleveland 6, Ohio
Attn: S Sesiy, Head

Dr C J Falbenbach
Battelle Memorial Institute
Columbus, Ohio
Attn: Electrical Engineering Division

Librarian
Engineering Library
Brown University
Providence, Rhode Island

Professor A W Straiton
Dept of Electrical Engineering
University of Texas
Austin 12, Texas

Mr William Way
Research Librarian
Technical Instruments Corp
3349 Cahuenga Boulevard
Hollywood 28, California

SOLID STATE ONLY

Martin A Caroiano, Head
Paramagnetic Section
Magnetism Branch
Solid State Division
Naval Research Laboratory
Washington 25, D C.
Attn: Code 6451

Dr. Reinier Beeuwkes, Jr
Ordnance Materials
Research Laboratory
Watertown Arsenal
Watertown, Massachusetts

Mr A Saiba
Nimeji Technical College
Nimeji, Japan

Electronics Research Laboratory
Division of Electrical Engineering
University of California
Berkeley 4, California
Attn: Librarian

Johns Hopkins University
34th and Charles Street
Whitehead Hall
Baltimore 18, Maryland
Attn: Mr. J. G. Armson

Librarian
Physics Department
Amherst College
Amherst, Massachusetts
Attn: Mr. Remer

Professor I. Lowe
Department of Physics
University of Minnesota
Minneapolis, Minnesota

Professor R. E. Norberg
Department of Physics
Washington University
St. Louis, Missouri

Microwave Research Institute
Polytechnic Institute of Brooklyn
55 Johnson Street
Brooklyn, New York
Attn: Librarian

Dr. Sidney Shapiro
Arthur D. Little, Inc
15 Acorn Park
Cambridge 40, Massachusetts

Dr. Simon Foner
Lincoln Laboratories
Box 73
Lexington, Massachusetts

Mr. William H. From
Ewen Knight Corporation
286 A Street
Needham, Massachusetts

Dr. Edward U. Condon
5644 Waterman Avenue
St Louis, Missouri

Dr. W. M. Walsh
Bell Telephone Labs., Inc
Murray Hill, New Jersey

Librarian
IBM Watson Laboratories
612 West 115th Street
New York 27, New York

ELECTROMAGNETIC RADIATION ONLY

Michigan State College
Department of Mathematics
East Lansing, Michigan

Microwave Research Institute
Polytechnic Institute of Brooklyn
55 Johnson Street
Brooklyn, New York

Mr. L E Swarts, Jr.
Building 12, Room 2417
Hughes Research Laboratories
Culver City, California

Professor O.E.H. Rydbeck
P. O. Box 246
Bolmar, New Jersey

One Copy Unless Otherwise Specified